Methodological problems in pressure profile calculations for lipid bilayers

Jacob Sonne,[a] Flemming Y. Hansen, and Günther H. Peters[a),b]
Department of Chemistry, Technical University of Denmark, DK-2800 Lyngby, Denmark

From molecular dynamics simulations of a dipalmitoyl-phosphatidyl-choline (DPPC) lipid bilayer in the liquid crystalline phase, pressure profiles through the bilayer are calculated by different methods. These profiles allow us to address two central and unresolved problems in pressure profile calculations: The first problem is that the pressure profile is not uniquely defined since the expression for the local pressure involves an arbitrary choice of an integration contour. We have investigated two different choices leading to the Irving–Kirkwood (IK) and Harasima (H) expressions for the local pressure tensor. For these choices we find that the pressure profile is almost independent of the contour used, which indicates that the local pressure is well defined for a DPPC bilayer in the liquid crystalline phase. This may not be the case for other systems and we therefore suggest that both the IK and H profiles are calculated in order to test the uniqueness of the profile. The second problem is how to include electrostatic interactions in pressure profile calculations when the simulations are conducted without truncating the electrostatic potential, i.e., using the Ewald summation technique. Based on the H expression for the local pressure, we present a method for calculating the contribution to the lateral components of the local pressure tensor from electrostatic interactions evaluated by the Ewald summation technique. Pressure profiles calculated with an electrostatic potential truncation (cutoff) from simulations conducted with Ewald summation are shown to depend on the cutoff in a subtle manner which is attributed to the existence of long-ranged charge ordering in the system. However, the pressure profiles calculated with relatively long cutoffs are qualitatively similar to the Ewald profile for the DPPC bilayer studied here. © *2005 American Institute of Physics.* [DOI: 10.1063/1.1862624]

I. INTRODUCTION

A system consisting of two or more phases will have interfacial regions that separate the bulk phases. The properties of interfacial regions can be characterized through macroscopic variables such as the surface tension, surface free energy, bending modulus, saddle splay modulus, etc. These properties can be determined from the pressure distribution through the interfacial region[1–3] (the pressure profile). Therefore, pressure profiles provide a microscopic interpretation of interfacial phenomena allowing, for instance, determination of the viscosity profile,[4,5] which is of great interest in materials and polymer science.

Pressure profiles are not available experimentally[6] but can be calculated from, e.g., molecular dynamics (MD) simulations (see, e.g., Refs. 7–11). Early MD studies of simple liquid-gas interfaces[7,8] explored methods for calculating the local pressure and provided insight into the microscopic properties of the surface tension. In biological systems, such as cell membranes, the pressure profile plays a central role since the function and survival of living cells is tightly coupled to the mechanical properties of the membrane.[12] Moreover, it has been suggested that the pressure profile in cell membranes undergoes changes in the presence of anesthetic compounds and that this change might be a key step in general anesthesia.[13,14] Changes in the pres-

sure profile in lipid bilayers, which is a common model system for cell membranes, has also been shown to affect the function of mechanosensitive channels.[11] Computer simulations[9–11,15] of lipid bilayers indicate that bilayers have regions with negative lateral pressure trying to minimize the interfacial area, and regions with positive lateral pressure trying to expand the bilayer. The mentioned MD bilayer studies, as well as less detailed models,[1,6,16] predict lateral pressure variations in these regions of several hundred bars.

In order to determine the pressure profile one needs to calculate the local pressure. The local pressure is not uniquely defined since the expression for the local pressure involves an integral along an arbitrarily chosen contour.[17] In previous studies, two contours have been employed leading to two different expressions for the local pressure tensor, namely, the Irving–Kirkwood[18] (IK) and the Harasima[19] (H) local pressure tensors. An obvious dilemma in pressure profile calculations is that it is not possible to rule in favor of either of these expressions. In most bilayer studies the IK expression has been preferred.[9–11,15]

The IK expression is applicable for interactions described by m-body potentials, where m is finite,[10] which makes it possible to include local pressure contributions from, e.g., valence angle and dihedral interactions. There is no problem in including electrostatic interactions when these are calculated directly from the Coulomb potential ($m=2$). For computational reasons, calculating electrostatic interactions directly from the Coulomb potential requires the use of

---

a)Member of MEMPHYS – Center for Biomembrane Physics.
b)Electronic mail: ghp@kemi.dtu.dk

122, 124903-1

a cutoff and due to the long-range nature of electrostatic interactions, the cutoff should be fairly long. However, even when the cutoff is long, structural artifacts may be introduced in the system[20,21] and therefore the use of an electrostatic potential cutoff is not always an optimal choice.[4] One way to avoid this is to evaluate the electrostatic interactions by the Ewald summation technique (see, e.g., Ref. 4), in which the electrostatic interactions are split up in a real and reciprocal space contribution. The real space contribution is still pairwise additive with $m=2$, while m is formally infinite in the reciprocal space sum. Consequently, it is not possible to include the contribution from the reciprocal space part of the Ewald sum in the pressure profile using the IK expression for the local pressure tensor. One approach[9,11] to this problem has been to calculate the pressure profile by the IK expression, using a long cutoff for the electrostatic interactions. When the simulations are conducted using a cutoff, the pressure profile should also be calculated using the same cutoff for consistency. However, when the simulations are conducted using Ewald summation while the pressure profile is calculated with a finite cutoff, the long-range electrostatic interactions are neglected in the latter calculation. The neglected contribution to the lateral pressure may be relatively small, but one should keep in mind, that the local lateral pressure may vary several hundred bars through the bilayer even though bulk pressure in the simulation is merely 1 bar.[9–11,15] Thus, a small contribution to the total simulation pressure might not be negligible in pressure profile calculations. A method for including the reciprocal space contribution was developed by Alejandre, Tildesley, and Chapela[8] in a study of a water-vapor interface. In this method, they used different expressions for the real space and reciprocal space electrostatic contributions to the pressure profile and their method was only set up to handle systems with one kind of molecules that were assumed to be rigid.

The present work addresses two central problems in pressure profile calculations. The first problem is the arbitrariness in the choice of integration contour. We will investigate this problem by comparing the pressure profiles obtained with the two different contours that lead to the IK and H expressions for the local pressure. The second problem is how to include the electrostatic contribution to the local pressure tensor when Ewald summation is used in a multicomponent system with flexible molecules.

The paper is organized as follows: First, in Sec. II, we summarize the theory of local pressure calculation and show how the H expression can be used to calculate the local pressure contribution from the Ewald sum evaluation of electrostatic interactions in systems with different and flexible molecular species. In Sec. III and the Appendix we describe the system setup and other simulation details. In Sec. IV A the differences between pressure profiles calculated according to the IK and H expressions are investigated for a dipalmitoylphosphatidyl-choline (DPPC) lipid bilayer. Based on these investigations, we discuss the uniqueness of the pressure profile for the system in consideration. In Sec. IV B, the pressure profile including all electrostatic interactions as determined by the Ewald summation technique is compared to pressure profiles calculated with varying cutoffs for the elec-

trostatic interactions. From this comparison, we discuss the long-range electrostatic contribution to the pressure profile. The results in Sec. IV B are followed by a summary and the conclusion.

II. THEORY

A. Bulk pressure tensor

The bulk pressure tensor for a system is a sum of kinetic and configurational contributions, i.e., $\mathbf{P}^{tot}=\mathbf{P}^{kin}+\mathbf{P}^{config}$. In this paper, only the configurational part of the pressure tensor is of interest and for simplicity it will be denoted $\mathbf{P}$. The $\alpha\beta$ element of the configurational part of the pressure tensor is obtained from the virial theorem,[4]

$$P^{\alpha\beta} = \left\langle \frac{1}{V}\sum_i f_i^\alpha r_i^\beta \right\rangle = \left\langle -\frac{1}{2V}\sum_{i\neq j} f_{ij}^\alpha r_{ij}^\beta \right\rangle, \tag{1}$$

where V is the volume of the system, $\mathbf{f}_i$ the total force on particle i and $\mathbf{r}_i$ its position. The brackets denote time averaging. In the second part of the equation we have used $\mathbf{r}_{ij}=\mathbf{r}_j-\mathbf{r}_i$ and have assumed that the interactions in the system may be written as a sum over pair interactions, that is, $\mathbf{f}_i=\sum_j' \mathbf{f}_{ij}$ where $\mathbf{f}_{ij}$ is the force on particle i due to particle j. The prime in the summation indicates that $j\neq i$.

B. Local pressure tensor

By setting up a microscopic momentum balance and relating this to the corresponding continuum expression one arrives at the following expression for the configurational part of the local pressure tensor:[7,17,22]

$$P^{\alpha\beta}(\mathbf{r}) = \left\langle \sum_i f_i^\alpha \int_{\mathcal{C}_{0i}} \delta[\mathbf{r}-\mathbf{l}]ds^\beta \right\rangle. \tag{2}$$

The contour integral runs along an arbitrary path $\mathcal{C}_{0i}$ from a reference position $\mathbf{R}_0$ to the position of the ith particle $\mathbf{r}_i$. $\mathbf{s}$ is a line element on $\mathcal{C}_{0i}$ and $\mathbf{l}$ is the position vector of the line element. $\delta[\mathbf{r}-\mathbf{l}]$ is the Dirac delta function. Equation (2) expresses that the pressure tensor near the point $\mathbf{r}$ is a sum of contributions coming from all particles $\{k\}$ for which the corresponding contours $\{\mathcal{C}_{0k}\}$ pass through the region around $\mathbf{r}$.

For a pairwise additive potential, Eq. (2) can be expressed as[2,7,17,22]

$$P^{\alpha\beta}(\mathbf{r}) = \left\langle -\frac{1}{2}\sum_{i\neq j} f_{ij}^\alpha \int_{\mathcal{C}_{ij}} \delta[\mathbf{r}-\mathbf{l}]ds^\beta \right\rangle. \tag{3}$$

In the derivation of Eq. (3) from Eq. (2), the contour $\mathcal{C}_{0i}$ is forced through $\mathbf{r}_j$ and the integral is split into an integral over $\mathcal{C}_{0j}$ minus an integral over $\mathcal{C}_{ij}$. The integral along $\mathcal{C}_{0j}$ is zero no matter how the contour is chosen due to the translational invariance of the forces, while the integral along $\mathcal{C}_{ij}$ in general depends on the path chosen.[10]

In the following we present the local pressure expressions based on two different choices of $\mathcal{C}_{ij}$. The expressions for the local pressure will be written for a system of planar geometry and will be discretized to slabs of finite size which makes the expressions suitable for implementation in a MD
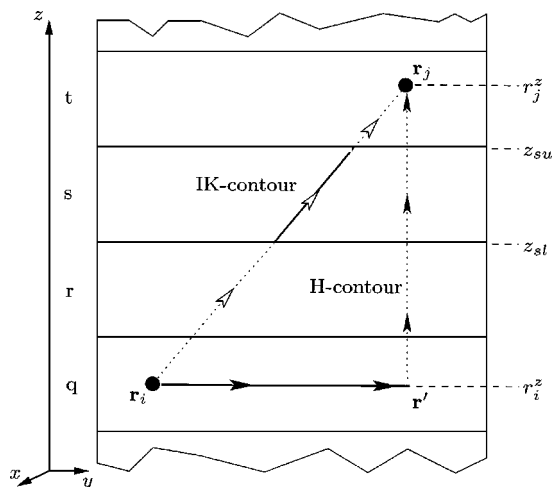
FIG. 1. Illustration of the contours leading to the IK and H expressions for the local pressure tensor (open and filled arrows, respectively). The bold part of the IK contour indicates the fraction of the full virial from the interaction between i and j that is assigned to slab s according to Eq. (4). The bold part of the H contour indicates that the virial of the interaction from i to j is assigned to slab q according to Eq. (6).

program. Note that the bulk pressure tensor in Eq. (1) is a simple average of the local pressures in all slabs. This is used as a consistency check of the calculations.

1. Irving–Kirkwood contour

The IK expression for the local pressure tensor[18] is obtained by choosing the contour $\mathcal{C}_{ij}$ as a straight line connecting the particle pair ij.[2,7,17,22] This contour (IK contour) is illustrated in Fig. 1 (open arrows). In planar geometry (rotational symmetry around the z axis) the configurational contribution to the lateral pressure, $P_L \equiv (P^{xx} + P^{yy})/2$, in slab s, extending from z_{sl} to z_{su} with volume V_s, is given by

$$P_L(s) = \left\langle -\frac{1}{2V_s}\sum_{i\neq j}\frac{f_{ij}^x r_{ij}^x + f_{ij}^y r_{ij}^y}{2}F_s(z_{su}, z_{sl}, r_i^z, r_j^z)\right\rangle, \quad (4)$$

where F_s is the fraction of the connecting line between i and j that is located within slab s, i.e., between z_{sl} and z_{su}. In Fig. 1, F_s is given by the ratio between the length of the bold part of the IK contour and the length of the full IK contour which can be expressed as

$$F_s = |z_{su} - z_{sl}|/|r_j^z - r_i^z|. \quad (5)$$

The expression in Eq. (4) can be generalized to m-body interactions with m finite[10] and it is therefore straightforward to include local pressure contributions from valence angles ($m=3$) and dihedral interactions ($m=4$). Electrostatic interactions can also be incorporated using Eq. (4) if all electrostatic interactions are evaluated directly from the Coulomb potential. However, using the Ewald summation technique[4] introduces a problem in the pressure profile calculation since the reciprocal space part of the sum can not be expressed as m-body interactions with m finite and it is therefore not possible to determine F_s in Eq. (5).
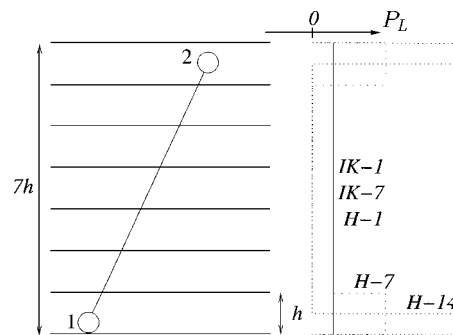

FIG. 2. Schematic illustration of the local pressure distribution coming from the IK and H expressions (solid and dotted lines, respectively) when varying the slab width. See text for details.

2. Harasima contour

The contour leading to the Harasima expression for the local pressure tensor[19] goes from particle i at $\mathbf{r}_i = r_i^x\hat{\mathbf{e}}_x + r_i^y\hat{\mathbf{e}}_y + r_i^z\hat{\mathbf{e}}_z$ to particle j at $\mathbf{r}_j = r_j^x\hat{\mathbf{e}}_x + r_j^y\hat{\mathbf{e}}_y + r_j^z\hat{\mathbf{e}}_z$ via straight lines through the intermediate point $\mathbf{r}' = r_j^x\hat{\mathbf{e}}_x + r_j^y\hat{\mathbf{e}}_y + r_i^z\hat{\mathbf{e}}_z$ (H contour, lines marked with filled arrows in Fig. 1). The resulting expression for the lateral pressure in slab s is[7,17,19,22]

$$P_L(s) = \left\langle -\frac{1}{2V_s}\sum_{i\neq j}\frac{f_{ij}^x r_{ij}^x + f_{ij}^y r_{ij}^y}{2}\right.$$
$$\left.\times\Theta(z_{su} - r_i^z)\Theta(r_i^z - z_{sl})\right\rangle, \quad (6)$$

where $\Theta(x)$ is the Heaviside step function. Equation (6) expresses that half of the lateral pressure arising from the interaction between i and j is assigned to the slab where i is located (cf. bold part of the H contour in Fig. 1). The other half of the lateral pressure from this pair is assigned to the slab where j is located.

3. Properties of the IK and H expressions

At this point we have two expressions for the local pressure and when m is finite both Eqs. (4) and (6) can be applied with almost equal simplicity. However, there are two important differences between the expressions that will be discussed in the following:

(1) The IK expression distributes the virial evenly on the connecting line between two interacting particles and therefore the contribution to the local pressure from this pair is the same in all slabs in the region between the two particles. Further, the local pressure is independent of the number of slabs when the slab width is smaller than the distance between the two particles (range of interaction) except for the slabs with the particles. There, the connecting line between the particles does not cross the entire slab. If the lateral contribution to the virial from this interaction is W_{12}, then the lateral pressures in all seven slabs are the same and equal to $\left(\frac{1}{7}W_{12}\right)/(Ah)$, where A is the xy area of the simulation box and h is the slab width. If we were using only one slab of height $7h$ (as indicated to the left in Fig. 2) the lateral pressure in this slab would also be $(W_{12})/(7Ah)$. To the right in Fig. 2 the corresponding pressure distributions are shown and the IK-1 and the IK-7 profiles (IK profile using 1 and 7

slabs, respectively) coincide. This property can also be seen from Eq. (4) where the slab volume V_s and the fraction of connecting line in the slab F_s both scale linearly in the slab width. Thus, the pressure in a slab is independent of the slab width. These simple considerations also indicate that, for one pair, the IK expression will not predict local pressure variations on length scales that are shorter than the relevant "range of interaction." Therefore, it is reasonable to use a slab width which is comparable to the shortest range of interaction.

The local pressure distribution from the H expression is also shown in Fig. 2. With one slab, the lateral pressure distribution, is identical to the IK profiles as illustrated by the H-1 profile. This illustrates that the local pressure is independent of the choice of contour and therefore well defined on the length scale of the range of interaction. This is true for any contour that is confined to the region between the particles. When the slab width is decreased to h, i.e., we are using seven slabs, the H expression gives the pressure $(\frac{1}{2}W_{12})/(Ah)$ in the two slabs where the particles are located and zero elsewhere (H-7 profile in Fig. 2). Increasing the number of slabs (thereby reducing the slab width) will cause the H pressure, in the two slabs with the particles, to increase which is illustrated by the H-14 profile in Fig. 2 (14 slabs between the particles). The pressure peaks in the H-profile can be smeared out by the motions of the two particles and for a homogeneous particle density, the IK and H profiles are identical.[17] The invariance of the local pressure to the slab width favors the use of the IK expression over the H expression, but does not imply that IK profiles are more correct.

(2) As described in Sec. II B 1, the IK expression cannot be used to calculate the local pressure contribution from the reciprocal space part of the Ewald sum. This is, however, possible with the H expression: If the virial from the interaction from particle i to particle j is known, one need not know r_j^z in order to use the H expression in Eq. (6). Although the reciprocal space sums are not expressed in terms of pair interactions, it is possible to derive an expression for the pressure contribution coming from interactions between particle i and all particles represented in the reciprocal space part of the Ewald sum (see the following section). This contribution can be considered as sum of many pairwise additive contributions (between i and different j's), which should all be assigned to the slab where i is located, and therefore the sum of these pair contributions can be assigned to the slab where i is located. This approach will be referred to as the Harasima–Ewald (HE) method.

Since the vertical part of the H contour (cf. Fig. 1) passes through all slabs between the interacting particles, like the IK contour, the zz element of the H pressure tensor depends on two particle positions in a similar way as the IK expression in Eq. (4) does. The expression for the zz element of the H local pressure tensor is obtained by substituting the superscripts x and y with z on f and r in Eq. (4).[7,17,22] Therefore, it is not possible to calculate this component of the local pressure tensor from electrostatic interactions evaluated by Ewald summation using the HE method. This, however, does not present a problem since the zz element of the local pressure tensor (including all interactions) is equal to the

bulk pressure everywhere in the simulation box for a system in mechanical equilibrium ($\nabla \cdot \mathbf{P} = 0$). The fact that the H expression allows the reciprocal space part of the Ewald sum to be included in the lateral pressure profile favors the H expression over the IK expression.

C. Ewald summation and local pressure

In the preceding section we argued that the H expression in Eq. (6) can be used for distributing the lateral pressure contribution from the reciprocal space part of the Ewald sum, if the pressure contribution from the interaction between particle i and all particles represented in the reciprocal space sums $\mathbf{P}_{K,i}$ is known. Such an expression is derived in the following.

Using periodic boundary conditions, the Coulomb energy U_C of N particles with partial charges $\{q\}$ and positions $\{\mathbf{r}\}$ can be expressed by the Ewald sum:[4]

$$U_C = \frac{1}{2V\epsilon_0} \sum_{k_n \neq 0} Q(k_n)S(\mathbf{k}_n)S(-\mathbf{k}_n)$$

$$+ \frac{1}{4\pi\epsilon_0} \sum_{i<j \in I} q_i q_j \mathrm{erfc}(\kappa r_{ij})/r_{ij}$$

$$- \frac{1}{4\pi\epsilon_0} \sum_{i<j \notin I} q_i q_j \mathrm{erf}(\kappa r_{ij})/r_{ij} - \frac{\kappa}{4\pi^{3/2}\epsilon_0} \sum_i q_i^2. \quad (7)$$

Here ϵ_0 is the vacuum permittivity, r_{ij} is the distance between particle i and j, and κ is a parameter that shifts the energy contribution from the real to the reciprocal space as κ increases. I is the list of particle pairs for which the energy is evaluated. erf is the error function and erfc is the complementary error function. V is the volume of the simulation box which, for an orthogonal box, is given by $V = L^x L^y L^z$ where L^α is the box length in the α direction ($\alpha = x, y, z$). $\mathbf{k}_n$ is the reciprocal lattice vector given by

$$\mathbf{k}_n = 2\pi(n^x/L^x, n^y/L^y, n^z/L^z)\begin{pmatrix} \hat{\mathbf{e}}_x \\ \hat{\mathbf{e}}_y \\ \hat{\mathbf{e}}_z \end{pmatrix}, \quad (8)$$

with $n^\alpha = 0, \pm 1, \pm 2, \pm 3, \ldots$. $S(\mathbf{k}_n)$ is given by

$$S(\mathbf{k}_n) = \sum_{j=1}^{N} q_j \exp(i\mathbf{k}_n \cdot \mathbf{r}_j), \quad (9)$$

with $i^2 = -1$. $Q(k_n)$ is given by

$$Q(k_n) = \exp(-k_n^2/4\kappa^2)/k_n^2. \quad (10)$$

Note that Eq. (7) assumes that κ has been chosen so that the real space part of the energy has converged within the central simulation box. In practice κ is chosen such that the real space energy converges within a specified distance that is smaller than half the length of the simulation box. The first term in Eq. (7) is the reciprocal space contribution U_K to the total Coulomb energy U_c. From U_K one can extract the energy $U_{K,i}$ of particle i due to all other particles represented in the reciprocal space sum. This energy satisfies $U_K = \frac{1}{2}\sum_i U_{K,i}$ and is given by[23]

$$U_{K,i} = \frac{q_i}{V\epsilon_0} \sum_{\mathbf{k}_n \neq \mathbf{0}} Q(k_n) \mathrm{Re}[\exp(-i\mathbf{k}_n \cdot \mathbf{r}_i) S(\mathbf{k}_n)]. \quad (11)$$

Here Re denotes the real part of the argument. For a rectangular simulation box, the diagonal elements of the instantaneous configurational contribution to the pressure tensor are given by[24,25] $P^{\alpha\alpha}V = -(\partial U/\partial L^\alpha)L^\alpha$. Using the energy expression in Eq. (11) gives the following expression for the instantaneous reciprocal space pressure contribution from particle i:

$$P_{K,i}^{\alpha\beta}V = \frac{q_i}{V\epsilon_0} \sum_{\mathbf{k}_n \neq \mathbf{0}} Q(k_n) \mathrm{Re}\big[\exp(-i\mathbf{k}_n \cdot \mathbf{r}_i) S(\mathbf{k}_n)\big]$$
$$\times \left[\delta_{\alpha\beta} - 2k_n^\alpha k_n^\beta \left(\frac{1}{k_n^2} + \frac{1}{4\kappa^2} \right) \right], \quad (12)$$

half of which should be assigned to the slab where particle i is located according to Eq. (6). $\delta_{\alpha\beta}$ in Eq. (12) is the Kronecker delta.

III. SIMULATION DETAILS

The lipid bilayer in the present study consists of 72 DPPC lipids solvated with 2000 water molecules resulting in a total of $\approx 16\,000$ atoms. The water molecules were placed around the bilayer using the program SOLVATE (by Grubmüller) and subsequently the water layer surrounding the bilayer was cropped to a rectangular, periodic simulation box with average xyz dimensions of $\approx 49 \times 45 \times 68$ Å^3. The water molecules were represented by the TIP3 water model.[26] The system was equilibrated for 15 ns with the area fixed to the experimental value (62.9 Å^2 as suggested by Nagle *et al.*[27]). Data for the pressure profile calculations were collected from the next 17 ns of propagation in the *N-P-T* ensemble. All simulations were carried out using the MD software NAMD (Ref. 28) with a time step of 1.0 fs. Both bonded and nonbonded interactions were updated every time step. The simulations were conducted at 300 K and an average isotropic pressure of 1 bar. The pressure was controlled by the Nosé-Hoover–Langevin barostat[29] with a piston oscillation time of 100 fs and a damping time of 50 fs. The three box lengths of the simulation box were allowed to adjust independently to the relevant pressure components. Electrostatic interactions were evaluated using the particle mesh Ewald (PME) method[30,31] with a grid spacing of less than 1 Å.

As recently demonstrated,[32] the CHARMM27 parameter set[33] does not reproduce the experimental value for the area per lipid or the experimental order parameter profile when the bilayer is allowed to adjust its area freely, as in the *N-P-T* ensemble. In the *N-P-T* ensemble the area per lipid is severely underestimated and is steadily decreasing in time.[32] Therefore, many membrane simulations using the CHARMM27 parameters are carried out in the *N-P-A-T* (*A* is the area of the bilayer in the *xy* plane) or *N-P_z-γ-T* (*γ* is the surface tension) ensembles.[11,15,32,34] The area per lipid can be adjusted to the experimental value in these ensembles, however, stretching the bilayer can introduce artifacts that are not easily recognized as such.[35,36] In the present study,
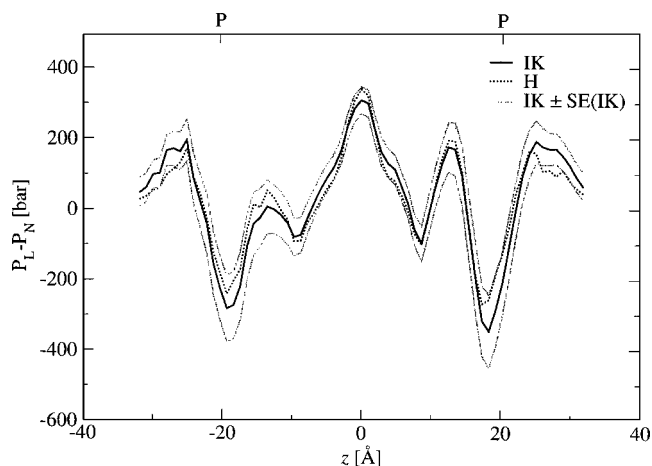

FIG. 3. Total pressure profiles from the IK and H expressions (four-point running average). Both are calculated with a cutoff of 20 Å for the electrostatic interactions. The z coordinate is defined normal to the bilayer with origin in the bilayer center of mass. To indicate the dimension of the bilayer, the z values corresponding to the maximal phosphorus density are marked with the letter P on the top axis of the graph. The solid gray lines show the upper and lower standard deviations [SE(IK)] of the average IK profile.

we have chosen to conduct all simulations in the *N-P-T* ensemble, using a new parameter set developed by the authors and coworkers (see Appendix).

Pressure profile calculations were carried out by postsimulation analysis of the trajectory using a program developed by the authors. The program uses routines from the programs MINDY[28] and CATDCD (developed by the Theoretical and Computational Biophysics Group, University of Illinois, Urbana-Champaign). The profiles were calculated with 70 slabs corresponding to an approximate slab width of 1 Å. The width was adjusted during the calculation according to the fluctuations in the size of the simulation box. In the following the z axis is defined as normal to the bilayer and $z=0$ is defined as the z component of the bilayer center of mass. The statistical analysis was carried out between data blocks averaged over 250 ps which were found to be uncorrelated.

IV. RESULTS AND DISCUSSION

A. Comparing IK and H pressure profiles

In this section we compare the pressure profiles obtained by the IK and H expressions. We have shown the total pressure profiles in Fig. 3 as calculated by the IK and H expressions with a electrostatic potential cutoff at 20 Å. In the pressure profile calculations the cutoff is limited to 20 Å, a restriction imposed by the box dimensions. Although it is possible to include the reciprocal space contribution in the H profile, we have chosen to use a finite cutoff to make a direct comparison with the IK profile possible. We note that both pressure profiles qualitatively resemble the profiles previously published from coarse grained,[10] united-atom,[9] and all-atom[11] models for lipid bilayers. The small asymmetry in the pressure profiles is probably caused by long wave length membrane undulations with correlation times of more than 5 ns.[36,37] For completeness we also include Fig. 4 that shows all five contributions to the H pressure profile in Fig. 3. From
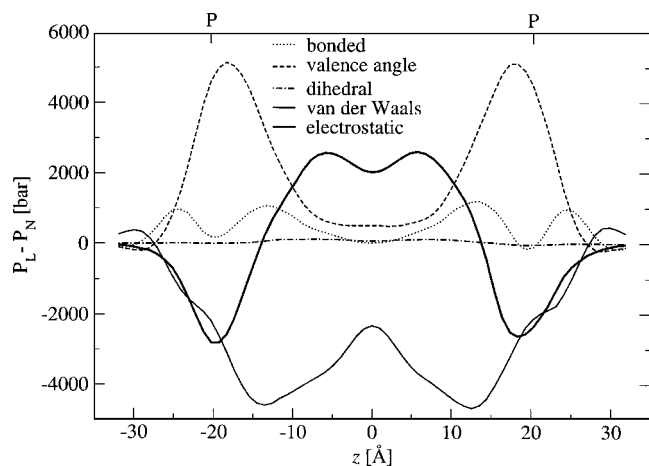
FIG. 4. Five pressure profile contributions calculated by the H expression for the bonded, valence angle, dihedral, van der Waals, and electrostatic interactions in a DPPC lipid bilayer (four-point running average). The sum of these contributions gives the total H pressure profile in Fig. 3. The z coordinate is defined normal to the bilayer with origin in the bilayer center of mass. To indicate the dimension of the bilayer, the z values corresponding to the maximal phosphorus density are marked with the letter P on the top axis of the graph.

FIG. 5. Total pressure profiles (four-point running average) calculated using cutoffs of 8, 12, 16, and 20 Å as well using HE method (Ewald). The maxima in the phosphorus density are marked with the letter P on the top axis of the graph. The standard error for all the pressure profiles is of the same magnitude as the standard error for the IK profile in Fig. 3.

Fig. 3 we see that the IK and H profiles deviate by less than ±50 bars in most regions and very importantly that the profiles have the same qualitative features. Pressure profiles calculated with electrostatic cutoffs at 8, 12, and 16 Å (not shown) give the same qualitative resemblance between the two ways of defining the local pressure. The similarity of the profiles in Fig. 3 suggests that the qualitative features of the pressure profiles for this system are rather insensitive to the choice of contour and therefore the pressure profile appears to be well defined, at least, within a margin of ±50 bars. The similarity between the IK and H profiles can probably be ascribed to the almost homogeneous particle density throughout the bilayer, with variations of only 10% from the average particle density. Since we only have demonstrated the invariance of the pressure profile to the choice of contour with the IK and H expressions for a DPPC lipid bilayer, we cannot claim the invariance to be universal. For example, in systems with density oscillations, such as liquids near a solid surface,[38] qualitative discrepancies between the IK and H pressure profiles have been reported.[39]

With that uncertainty in mind, we recommend that the pressure profile in a given system be calculated using both the IK and H expressions to check the uniqueness of the profile. Computing both profiles will not add significantly to the computation time.

Note that if we are only interested in calculating the surface tension γ for an interface [$\gamma = \int_{-L_z/2}^{L_z/2}(P_N - P_L)dz$], the IK and H expressions will always give the same result.[7,17] Therefore, irrespective of the nature of the system, the surface tension can be rigorously estimated from the pressure profile.

B. Cutoff versus Ewald summation

In the preceding section we concluded that the pressure profiles obtained from the IK and H expressions are qualita-
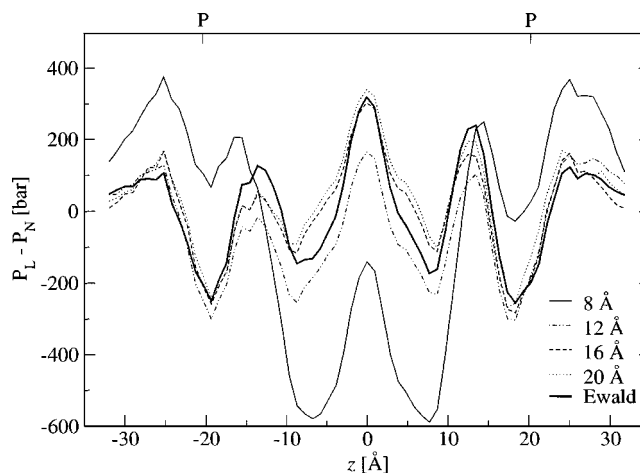
tively similar using cutoffs ranging from 8 to 20 Å. When the Ewald summation technique is used, the energy can no longer be expressed in terms of m-body interactions with m finite as discussed in Sec. II B 3, and the electrostatic contributions to the lateral pressure can therefore only be obtained by the H expression (using the HE method cf. Sec. II B 3). As long as the IK and H expressions lead to the same pressure profile, the HE method allows us to make a unique determination of the pressure profile when the Ewald summation technique has been used in the simulations. In the following, pressure profiles calculated by the HE method will be referred to as Ewald profiles.

As for the electrostatic energy calculated by the Ewald summation technique, the pressure profile should be independent of κ, i.e., independent of how the calculation of the profile is partitioned between the real and reciprocal spaces. Thus, we compared two Ewald profiles calculated with $\kappa = 0.14$ Å^{-1} and $\kappa = 0.40$ Å^{-1} (data not shown). At $\kappa = 0.14$ Å^{-1}, the reciprocal space contribution to the total electrostatic pressure is very small, whereas it accounts for 9% at $\kappa = 0.40$ Å^{-1}. Still, the $\kappa = 0.14$ Å^{-1} and $\kappa = 0.40$ Å^{-1} profiles are identical in all regions, which indicates that the HE method correctly deals with electrostatic pressure contributions evaluated by Ewald summation.

Then let us compare the pressure profiles obtained with the HE method and with different cutoffs of the electrostatic potential. The profiles are based on the 17 ns simulation where the PME technique was used. Figure 5 shows the total pressure profiles ($P_L - P_N$) calculated using cutoffs of 8, 12, 16, and 20 Å as well as the Ewald profile. Note that the pressure in the aqueous phase ($|z| > 26$ Å) is not isotropic in any of the profiles, which indicates that the simulation does not contain enough water for the aqueous phase to obtain bulk properties away from the bilayer. In Fig. 5 we see that the profile obtained with a cutoff of 8 Å deviates from the Ewald profile by up to −400 bars in the aliphatic part of the bilayer ($|z| < 14$ Å), and in the aqueous phase ($|z| > 26$ Å) the deviations amount to about 100 bars. One expects that by
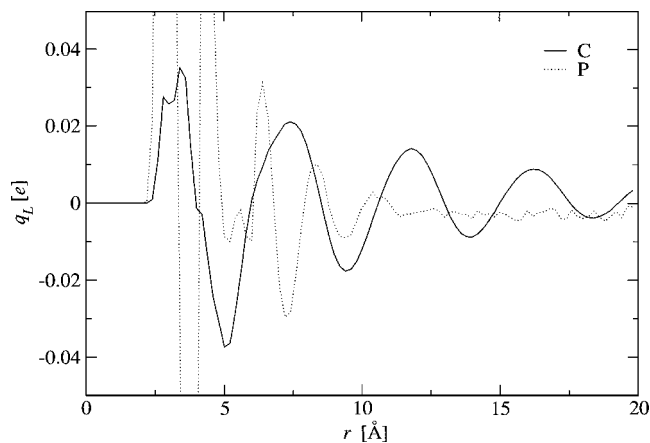
FIG. 6. The solid line is the lateral radial charge profile measured from aliphatic carbon atoms ($|z| < 14$ Å). The dotted line is the lateral radial charge profile measured from phosphorus atoms in the region 24 Å $< |z|$ < 16 Å. See text for details. As in the simulations, the electrostatic interactions between atoms that interact through covalent bonds or valence angle interactions were excluded in the calculation of the lateral charge profile.

increasing the cutoff, thereby including electrostatic interactions at larger distances, the cutoff profiles will approach the Ewald profile. This is indeed the case in all regions when the cutoff is increased from 8 to 12 Å, but surprisingly, Fig. 5 also shows that increasing the cutoff further to 16 and 20 Å causes an increase in the deviations from the Ewald profile in some regions, while other regions show only small deviations. Thus, the electrostatic pressure profile does not simply converge, in a monotonic fashion as the cutoff is increased. The pressure profiles in Fig. 5 result in surface tensions γ of 20 ± 6 mN/m (cutoff 8 Å), 28 ± 4 mN/m (cutoff 12 Å), -8 ± 4 mN/m (cutoff 16 Å), -22 ± 4 mN/m (cutoff 20 Å), and -6 ± 2 mN/m (Ewald). The surface tension is calculated using $\gamma = \int_{-L^z/2}^{L^z/2} (P_N - P_L) dz$ and the standard error for the average surface tension is estimated from the surface tensions in the uncorrelated 250 ps time blocks. These values also reflect the nonmonotonic convergence behavior in the system. A similar cutoff dependence is found for the energy of an ionic crystal, where it is well known that the electrostatic energy oscillates strongly as the cutoff is increased due to radial charge ordering. The analogy to ordered ionic structures is substantiated by the existence of a nonuniform lateral charge profile $q_L(r)$ in the bilayer (cf. Fig. 6). The lateral charge profile at $r = r'$, calculated for any reference atom, gives the total charge in a cylindrical slab of height h, extending laterally from r' to $r' + \delta r$ away from the reference atom. Thus, oscillations in $q_L(r)$ indicate lateral (or "in-slab") charge ordering in the system, which suggests that the energy and pressure from in-slab interactions will oscillate with increasing cutoff. In Fig. 6 the solid line shows the average lateral charge profile calculated for aliphatic carbon atoms with $|z| < 14$ Å. In the calculation of $q_L(r)$ the region $|z| < 14$ Å was divided into 14 slabs of width 2 Å and for all carbons in each slab, $q_L(r)$ was calculated with contributions from all other atoms in the slab. In each slab the $q_L(r)$'s around all carbon atoms were averaged to give one $q_L(r)$ for that slab and these $q_L(r)$'s were then averaged over the 14 slabs to give the solid line in Fig. 6. The figure shows that

the bilayer possesses lateral charge ordering which persists over the whole range considered. This explains why the cutoff profiles converge toward the Ewald profile in an oscillatory manner as seen in Fig. 5. Although in-slab electrostatic interactions give an important lateral pressure contribution since the lateral components of both $\mathbf{f}_{ij}$ and $\mathbf{r}_{ij}$ are relatively large and the whole pressure is assigned to one slab, the "out-of-slab" electrostatic interactions may also have significant lateral components that are governed by $q_L(r)$ in other slabs. The dotted line in Fig. 6 shows $q_L(r)$ for phosphorus calculated in the region 24 Å $< |z| < 16$ Å using a slab width of 2 Å. Comparing $q_L(r)$ for aliphatic carbon atoms with $q_L(r)$ for phosphorus atoms (Fig. 6 solid and dotted lines, respectively) we see that $q_L(r)$ varies through the bilayer, which is reflected in the quite complex cutoff dependence of the pressure profile. Adding to the complexity of the cutoff dependence of the pressure profile, one should keep in mind that the out-of-slab contributions also contribute to P_N. These may add or cancel contributions in P_L and therfore, the cutoff dependence of $P_L - P_N$ may be different from the one of P_L.

Note that $q_L(r)$ for phosphorus converges towards a negative charge, which means that the charge density in the phosphorus-rich region of the bilayer is negative. This indicates a nonuniform charge density in the direction normal to the bilayer giving rise to the electrostatic potential profile (see, e.g., Refs. 40 and 41).

We have found that increasing the electrostatic cutoff will not necessarily make the cutoff-profile approach the Ewald profile. This behavior can be explained in terms of charge ordering in the system which, as for ordered ionic systems, means that the results are sensitive to the cutoff distance. By using, e.g., charge-group based cutoff one can accommodate for some of the shortcomings of the brute force cutoff method. The charge-group based cutoff method would be straightforward to implement in pressure profile calculations both for the IK and H expressions, and would, in effect, damp the oscillations in the lateral charge profile. Therefore, pressure profiles calculated using the charge-group based cutoff are expected to be less cutoff dependent compared to the brute force cutoff profiles. A thorough investigation of different methods for treating electrostatic in MD simulations was carried out by Anézo et al.[42]

We would like to emphasize that although the cutoff profiles in Fig. 5 deviate from the Ewald profile, all the qualitative features of the Ewald profile are conserved in the cutoff profiles when using a reasonably long electrostatic potential cutoff (here 16 and 20 Å). However, since the simulation is conducted with Ewald summation, the cutoff profiles are approximations to the Ewald profile. Thus, even though we have found that pressure profiles in the DPPC lipid bilayer, calculated with a long cutoff from Ewald simulations, are qualitatively correct, other systems may have a different charge structure and therefore may have a different cutoff dependence which is not known a priori.

V. CONCLUSION

In this paper we have addressed two central issues concerning pressure profile calculations, namely, the arbitrariness in the choice of integration contour and the treatment of long-range electrostatic interactions.

Regarding the choice of integration contour we find that the Irving–Kirkwood (IK) and Harasima (H) expressions give qualitatively very similar pressure profiles for a DPPC lipid bilayer. The deviations between the IK and H profiles are below ±50 bars in most regions. However, in systems with strong density oscillations, such as liquids close to a wall, it has been reported that the IK and H pressure profiles have regions where they deviate qualitatively.[39] Therefore, in such regions, the local pressure is not uniquely defined and a detailed interpretation of the local pressure must be encumbered with great uncertainty. Thus, with a given system, a comparison of the pressure profiles obtained by the IK and H expressions is advisable in order to check the uniqueness of the pressure profile.

Concerning the treatment of long-range electrostatic interactions, we have shown how the H expression for the local pressure can be used to include the electrostatic contributions to the lateral components of the local pressure tensor calculated from the Ewald sum through the so-called Harasima–Ewald method (HE method). We used the HE method to calculate pressure profiles for a DPPC lipid bilayer and the pressure profile is found to be independent of the partitioning between the real space and the reciprocal space contributions to the Ewald sum.

The pressure profile can also be calculated using a finite cutoff for the electrostatic interactions. This approach is consistent if the simulations are also conducted with the same cutoff, but if the simulations are conducted using Ewald summation, such a pressure profile is inconsistent. The effect of this inconsistency was investigated by comparing pressure profiles calculated with different electrostatic potential cutoffs (8, 12, 16 and 20 Å) with the Ewald profile. We found that the cutoff profiles approach the Ewald profile in a nonmonotonic fashion which was attributed to the existence of long-range charge ordering in the bilayer. Even though the variations in the pressure profile with cutoff are found to be rather subtle, the qualitative features of the cutoff profiles are similar to the Ewald profile when a relatively large cutoff is used (16 and 20 Å). Further, considering the uncertainty in the pressure profile caused by the arbitrariness in the choice of integration contour, the deviations between the cutoff profiles and the Ewald profile are not serious as long as a relatively long cutoff is used. However, other systems may have a different charge structure compared to a DPPC bilayer and therefore the cutoff dependence of the pressure profile may be different.

For systems that are simulated using Ewald summation, the HE method can be used for pressure profile calculation without investigating the cutoff dependence of the pressure profile, regardless of the charge structure in the system. Thus, calculating the pressure profile by the HE method has great advantages compared to calculations using an electrostatic potential cutoff.
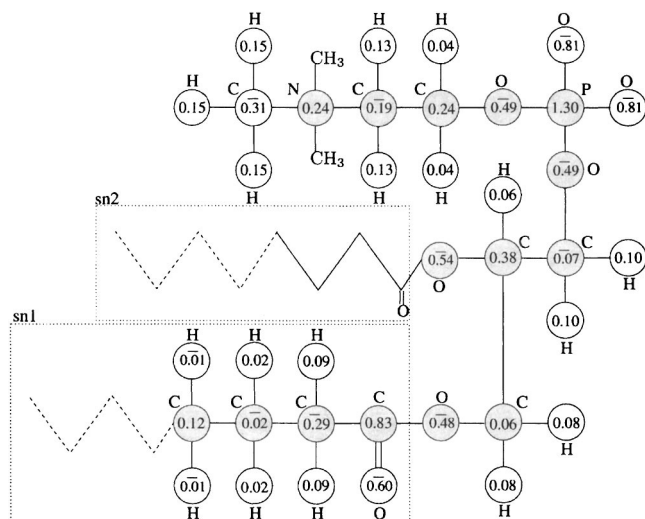

FIG. 7. Partial charges for the DPPC lipids in the simulation. The atoms in the lipid "backbone" are drawn in gray. The atoms in the three methyl groups on nitrogen have identical charges but for clarity only one methyl group is shown explicitly. The solid zigzag line in the sn2 chain indicates that these atoms have been assigned new charges that are equal to the corresponding charges in the sn1 chain. For clarity, the atoms are only shown explicitly in the sn1 chain. The dashed lines in the sn1 and sn2 chains symbolize the rest of the acyl chain where the CHARMM27 charges were used. An over-bar indicates that the charge is negative.
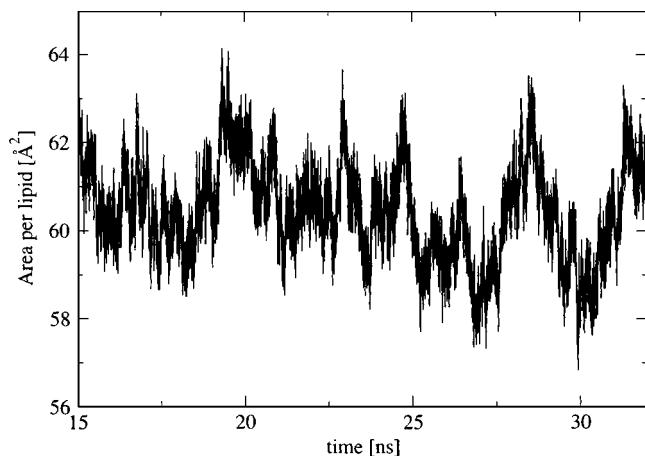
FIG. 8. The area per lipid as a function of time. Note that there is no drift in the area per lipid and that the average area is 60.4 Å². The data were obtained using a new lipid parameter set developed by the authors and co-workers.

APPENDIX: LIPID PARAMETERS

A new set of partial charges for the lipid head group was determined by *ab initio* calculations on 72 lipid configurations. The 72 lipid configurations were taken from an MD simulation with the area fixed to the experimental value. The average charges from these calculations was used in the present work and are presented in Fig. 7. The new parameter set gives an average area per lipid of 60.4 Å^2 (cf. Fig. 8) which is relatively close to the experimental value of 62.9 Å^2 considering the variations in the area per lipid as determined from different experiments.[43] The area per lipid is also in excellent agreement with the results of other simulations (using other forcefields): Berger, Edholm, and Jahnig[40] find 61.1 Å^2 and Tieleman and Berendsen[41] find 60.0 Å^2. Figure 8 indicates that the new DPPC bilayer serves as a good model system for testing the importance of long-range electrostatics in pressure profile calculations for lipid bilayers.

Further details on the methods used in the determination of the partial charges in Fig. 7 as well as an investigation of the bilayer properties will be published in the near future.

[1] I. Szleifer, D. Kramer, A. Ben-Shaul, W. M. Gelbart, and S. A. Safran, J. Chem. Phys. **92**, 6800 (1990).

[2] J. S. Rowlinson and B. Widom, *Molecular Theory of Capillarity* (Dover, New York, 2002).

[3] A. S. Safran, *Statistical Thermodynamics of Surfaces, Interfaces, and Membranes* (Addison-Wesley, Reading, MA, 1994).

[4] M. P. Allen and D. J. Tildesley, *Computer Simulations of Liquids* (Clarendon, Oxford, 1987).

[5] M. Ø. Jensen, O. G. Mouritsen, and G. H. Peters, Phys. Rev. E **64**, 1 (2001).

[6] D. Marsh, Biochim. Biophys. Acta **1286**, 183 (1996).

[7] J. P. R. B. Walton, D. J. Tildesley, J. S. Rowlinson, and J. R. Henderson, Mol. Phys. **48**, 1357 (1983).

[8] J. Alejandre, D. J. Tildesley, and G. A. Chapela, J. Chem. Phys. **102**, 4574 (1995).

[9] E. Lindahl and O. Edholm, J. Chem. Phys. **113**, 3882 (2000).

[10] R. Goetz and R. Lipowsky, J. Chem. Phys. **108**, 7397 (1998).

[11] J. Gullingsrud and K. Schulten, Biophys. J. **85**, 2087 (2003).

[12] D. Boal, *Mechanics of the Cell* (Cambridge University Press, Cambridge, 2002).

[13] R. S. Cantor, Biochemistry **36**, 2339 (1997).

[14] R. S. Cantor, Biophys. J. **82**, 2520 (2002).

[15] J. Gullingsrud and K. Schulten, Biophys. J. **86**, 3496 (2004).

[16] J. N. Israelachvili, S. Marcelja, and R. G. Horn, Q. Rev. Biophys. **13**, 121 (1980).

[17] P. Schofield and J. R. Henderson, Proc. R. Soc. London, Ser. A, **379**, 231 (1982).

[18] J. H. Irving and J. G. Kirkwood, J. Chem. Phys. **18**, 817 (1950).

[19] A. Harasima, Adv. Chem. Phys. **1**, 203 (1958).

[20] W. F. Van Gunsteren and A. E. Mark, J. Chem. Phys. **108**, 6109 (1998).

[21] M. Patra, M. Karttunen, M. T. Hyvonen, E. Falck, P. Lindqvist, and I. Vattulainen, Biophys. J. **84**, 3636 (2003).

[22] J. P. R. B. Walton and K. F. Gubbins, Mol. Phys. **55**, 679 (1985).

[23] D. M. Heyes, Phys. Rev. B **49**, 755 (1994).

[24] S. Nosé and M. L. Klein, Mol. Phys. **50**, 1055 (1983).

[25] D. Brown and S. Neyertz, Mol. Phys. **84**, 577 (1995).

[26] W. L. Jorgensen, J. Chandrasekhar, J. D. Madura, R. W. Impey, and M. L. Klein, J. Chem. Phys. **79**, 926 (1983).

[27] J. F. Nagle, R. Zhang, S. Tristram-Nagle, W. Sun, H. I. Petrache, and R. M. Suter, Biophys. J. **70**, 1419 (1996).

[28] L. Kale, K. Schulten, R. Skeel, M. Bhandarkar, R. Brunner, A. Gursoy, N. Krawetz, J. Phillips, A. Shinozaki, and K. Varadarajan, J. Comput. Phys. **151**, 283 (1999).

[29] S. E. Feller, Y. Zhang, R. W. Pastor, and B. R. Brooks, J. Chem. Phys. **103**, 4613 (1995).

[30] T. Darden, D. York, and L. Pedersen, J. Chem. Phys. **98**, 10089 (1993).

[31] U. Essmann, L. Perera, M. L. Berkowitz, T. Darden, Hsing Lee, and L. G. Pedersen, J. Chem. Phys. **103**, 8577 (1995).

[32] M. Ø. Jensen, O. G. Mouritzen, and G. H. Peters, Biophys. J. **86**, 3556 (2004).

[33] S. E. Feller and A. D. MacKerell, Jr., J. Phys. Chem. B **104**, 7510 (2000).

[34] S. E. Feller and R. W. Pastor, J. Chem. Phys. **111**, 1281 (1999).

[35] D. P. Tieleman, S. J. Marrink, and H. J. C. Berendsen, Biochim. Biophys. Acta **1331**, 235 (1997).

[36] S. J. Marrink and A. E. Mark, J. Phys. Chem. B **105**, 6122 (2001).

[37] E. Lindahl and O. Edholm, Biophys. J. **79**, 426 (2000).

[38] J. N Israelachvili, *Intermolecular and Surface Forces* (Academic, New York, 1991).

[39] F. Varnik, J. Baschnagel, and K. Binder, J. Chem. Phys. **113**, 4444 (2000).

[40] O. Berger, O. Edholm, and F. Jahnig, Biophys. J. **72**, 2002 (1997).

[41] D. P. Tieleman and H. J. C. Berendsen, J. Chem. Phys. **105**, 4871 (1996).

[42] C. Anézo, A. H. de Vries, H.-D. Holtje, D. P. Tieleman, and S.-J. Marrink, J. Phys. Chem. B **107**, 9424 (2003).

[43] J. F. Nagle and S. Tristram-Nagle, Biochim. Biophys. Acta **1469**, 159 (2000).